Journal of Applied Fluid Mechanics, Vol. 17, No. 5, pp. 989-1001, 2024.
Available online at www.jafmonline.net, ISSN 1735-3572, EISSN 1735-3645.
https://doi.org/10.47176/jafm.17.05.2302

Examining the Uniformity of Flow Distribution in Manifolds

F. Yazici[1], M. A. Karadag[1], P. Gokluberk[1] and A. Kibar[2†]

[1] *Tamsan Bağlantı Elemanları A.Ş., Kocaeli, 41400, Turkey*
[2]*Mechanical and Material Technologies, Kocaeli University, Uzunciftlik Nuh Cimento Campus, Kocaeli, 41180, Turkey*

[†]*Corresponding Author Email: alikibar@kocaeli.edu.tr*

BSTRACT

Flow distribution uniformity in manifolds is important in various engineering applications. In this study, the effect of manifold design on flow distribution is examined using both experimental and numerical methods. A comparison was made between a straight manifold and a gradually decreasing cross-sectional design considering two different inlet diameters. In addition, the staggered manifold case with the most homogeneous outlet was compared with the conical manifold under the same conditions. The results demonstrate that the gradually decreasing manifold design significantly improves the flow rate uniformity compared with the straight manifold. This improvement is achieved by reducing the flow rate differences between the distribution branches, leading to a more balanced fluid distribution. The gradual reduction in the cross-sectional area allows the fluid to traverse at lower velocities in regions with higher resistance, effectively minimizing flow rate discrepancies and pressure drops. In addition, the effect of varying the inlet diameter on flow rate uniformity was investigated, revealing that larger inlet diameters contribute to improved flow distribution. The outlet uniformity of the staggered manifold matches the effective performance of the conical manifold, demonstrating similar performance at a lower cost. The results highlight the importance of designing an appropriate manifold, considering factors such as inlet diameter, channel geometry, and staggered ratio, to achieve efficient and uniform fluid distribution.

Article History

Received September 13, 2023
Revised December 9, 2023
Accepted December 11, 2023
Available online February 24, 2024

Keywords:

Hydraulic systems
Manifold
Flow distribution
Numerical simulation
Flow uniformity

1. INTRODUCTION

Manifolds are useful tools used in various industrial fields, including the construction, agriculture, and automotive industries. They are designed to divide fluid flows into multiple streams or to combine several streams into a single flow. Therefore, they optimize not only the flow rates but also the pressure and temperature effectively, enabling efficient distribution to various components. Manifolds contribute to increased system efficiency, reduced energy consumption, and prevention of component damage (Zhang et al., 2020).

As shown in Fig. 1, there are four main types of manifolds, each with unique applications: distributor, collector, parallel, and counterflow (Wang, 2011; Hassan et al., 2014a; Tomor & Kristóf, 2016). Distributor manifolds regulate flow rates and direct fluids to various system components, whereas collector manifolds combine flow from multiple sources into a single outlet. These two types are widely used in the chemical, mechanical, automotive, and hydraulic industries.

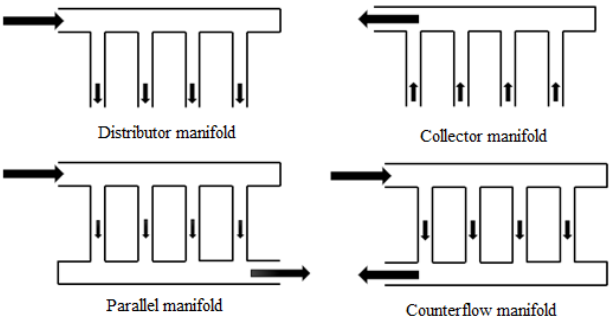

Fig. 1 Manifold types

Parallel manifolds are fluid distribution systems designed to distribute flow to multiple outlets with equal flow rates throughout the system. They are widely used in industries such as chemical, heating and cooling systems, air-powered systems, and liquid power applications where the distribution of liquids is important. The simple and efficient design of parallel manifolds ensures balanced flow distribution, maintaining consistent pressure and flow rates across the network (Wang et al., 2023). On the

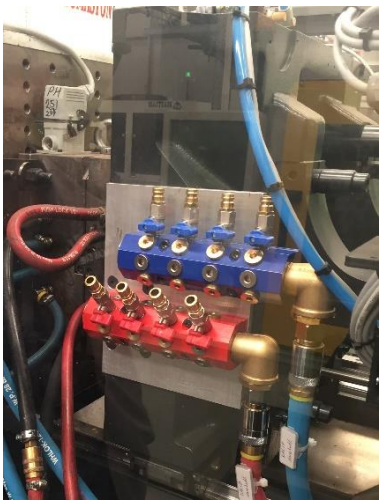

Fig. 2 Distributor manifold employing mold cooling

other hand, counter flow manifolds direct fluid in opposite directions in adjacent channels, facilitating efficient fluid mixing and heat transfer. Manifolds are commonly used in heat exchangers, chemical reactors, and cooling systems. Their unique design enhances thermal efficiency by promoting effective heat exchange between fluids with opposing flow directions (Kee et al., 2011; Mazaheri et al., 2022).

In hydraulic systems, manifolds maintain consistent pressure levels, ensuring that the flow is evenly distributed throughout the system components. It is important to consider fluid properties including flow rates, pressure, and temperature in the design of manifolds. The goal is to achieve efficient fluid distribution, minimize pressure drop, and enhance energy efficiency by optimizing channel geometry. High-performance hydraulic systems rely heavily on proper manifold design to ensure reliability and optimal operation. Incorrect or suboptimal designs can lead to various issues, including uneven flow distribution, pressure losses, and potential system failures.

Distributor block manifolds, which are employed for temperature control in molds, offer a straightforward, cost-effective, and optimized solution, particularly in environments where frequent mold changes are necessary. They route cooling water lines between the injection molding machine and the molds. Figure 2 shows an example of a distributor block manifold used for mold cooling. This manifold serves to route cooling water lines between the injection molding machine and the molds. Manufacturers prioritize achieving an equal pressure drop in each branch of the fluid after it leaves the manifold. To ensure this, it is crucial to connect the manifold close to the mold using short hoses, to minimize pressure and temperature losses in each arm. However, when the fluid flow rate varies from each branch, an uncontrolled pressure and thus temperature control situation may arise between the manifold and the mold. Consequently, temperature deviations in the mold increase, and maintaining a uniform temperature in the mold becomes challenging.

Manifolds facilitate the connection between hydraulic actuators (such as valves and cylinders) and pumps, making it easier to direct fluid flow. This allows hydraulic systems to operate efficiently while minimizing energy losses. Furthermore, manifolds help maintain the pressure balance within the system by controlling the pressure drop in the fluid flow. In addition, the design, material, and quality of the manifold component affect pressure loss and system performance (Zhang et al., 2018).

The flow distribution and pressure drops in a manifold system are influenced by two opposing forces: viscous friction and momentum (Acrivos et al., 1959; Minocha & Joshi, 2020; Tarodiya et al., 2020). Friction arises from fluid viscosity and interaction with solid walls, resulting in energy dissipation and pressure drops. In contrast, momentum effects come into play at the branching regions of the manifold system, where changes in flow direction occur (Minocha & Joshi, 2020). Viscous friction consumes the energy of the fluid, typically resulting in a pressure drop. However, branching of flow in a manifold or pipeline can lead to loss of momentum. The principle of momentum conservation indicates that this loss of momentum results in an unusable force and consequently causes a pressure drop. When the fluid divides into multiple flow paths or its velocity decreases, the momentum of the fluid also decreases. According to the law of conservation of momentum, pressure increases as fluid momentum decreases. Therefore, the pressure increases in regions where the fluid slows down, leading to a pressure drop. Consequently, the pressure drop within a manifold system is influenced by the combined effects of friction and momentum change (Minocha & Joshi, 2020).

Several studies have investigated the flow distribution in manifold systems and optimized pressure control. Bajura (1971) developed a theoretical model to investigate the flow distribution in the inlet and outlet manifolds of single-phase flow. The model was based on the principle of momentum conservation and focused on determining the optimal outlet angle on the lateral surfaces relative to the incoming flow. Subsequently, Bajura and Jones (1976) further enhanced this model, creating a framework that calculates flow velocities and pressures at lateral outlets in collector, distributor, parallel, and reverse flow manifolds. Jiang et al. (2022) conducted an experimental study to examine the impact of the area ratio and Reynolds number on the flow and pressure distribution in a distributor manifold. They concluded that controlling the flow rate is an effective approach for achieving homogeneous flow and pressure distribution. Furthermore, they highlighted that reducing the flow rate significantly improves performance.

Hassan et al. (2015) investigated the dependence of the flow distribution in manifolds on the arrangement, inlet pressure and inlet flow rate. Experimental and numerical models were used to investigate the flow uniformity of manifolds with different configurations. The results confirmed the efficiency of non-uniform diameter in fluid distribution, with the flow from the tapered cross-section manifold outlets being nearly uniform compared with that from the circular cross-section outlets, which showed severe maldistribution. A numerical model predicted the flow rates from the manifold laterals at

various Reynolds numbers, showing consistent trends with the experimental data. The Reynolds number had a slight effect on the uniformity of flow from outlets of the manifold, indicating that the flow distribution from manifold laterals is not influenced by the Reynolds number (Hassan et al., 2015).

Hassan et al. (2014b) studied flow homogeneity in manifold systems by narrowing the cross-section of the main pipe along its length. The study revealed that the flow rate at the lateral outlets remained consistent, regardless of whether the cross-section of the pipe gradually narrowed or remained unchanged. This finding indicated that the flow rate and distribution at the lateral outlets were independent of the Reynolds number. In a similar vein, Zhou et al. (2018) addressed the issue of flow imbalance in central-type parallel flow heat exchanger manifolds by modifying the insertion length of the pipes. By adjusting the insertion length, they successfully mitigated flow unevenness within the manifold. Karali et al. (2022) investigated the impact of tapered longitudinal section manifolds on a Z-shaped flat plate solar collector by examining the uniformity of flow distribution, pressure drop, and temperature profiles using a 3D model. The study highlighted that the tapered manifold improved the flow distribution, with an optimal taper ratio identified for each Reynolds number.

In the study of compact parallel manifolds in flow heat exchangers, flow maldistribution due to pressure maldistribution poses a challenge. Zhou et al. (2018) proposed a method involving the adjustment of insert lengths within the manifold to improve flow distribution uniformity. Numerical analysis was conducted on three different base cases with varying header diameters, demonstrating an average reduction in maldistribution by 72-82% while increasing pressure loss by 2.83%–6.46%. Despite the associated increase in pressure loss, the method effectively improved flow distribution uniformity across all flow rates. Wang et al. (2011) examined the liquid flow distribution in a small parallel flow heat exchanger using a rectangular inlet header and five modified versions (multi-step, trapezoidal, one baffle tube and two baffle plates). The flow distribution in the header is influenced by vortices generated by a jet stream at the inlet, resulting in uneven flow distribution in the front tubes. Among the modifications, the baffle tube demonstrates the most effective improvement in flow distribution by eliminating vortex flow, making it suitable for all flow rates.

Hassan et al. (2012) investigated the impact of outlet lengths on the lateral surfaces of a manifold system on flow distribution. They varied the length of the lateral surface outlets, starting with twice the diameter of the main pipe and then increasing to four and six times the diameters. The researchers found that increasing the length of the lateral surface outlets resulted in a more homogeneous flow distribution at the outlets. In a numerical study by Choi et al. (1993), the focus was on examining the effect of the cross-sectional area ratio between the main channel (where the flow enters the manifold in a liquid cooling module) and the lateral surface channels (where the flow exits). According to the findings, the flow rate of the frontmost outlet channel was approximately three times higher than that of the last outlet channel. This demonstrated that the ratio of the cross-sectional areas between the inlet and outlet channels is an important parameter influencing the flow distribution.

Korkmaz et al. (2021) conducted experimental and numerical investigations of the pressure drop in a banjo elbow with inlet characteristics similar to those of a manifold. They emphasized the importance of considering arm conditions coinciding with the inlet while connecting the banjo elbow, which significantly affects the pressure drop. Siddiqui et al. (2020) conducted flow distribution measurements on U-type and Z-type manifolds using particle imaging velocimetry (PIV) techniques. In U-type manifolds, higher flow rates were observed in channels near the inlet, whereas Z-type designs exhibited flow concentrations in regions close to the outlet. Manipulating the inlet flow velocity enhanced the flow distribution in the U-type designs, whereas the Z-type designs exhibited a nondispersive effect.

The main objective of this study is to investigate the flow behavior of manifolds and analyze their performance under different conditions. Numerical simulations were conducted and validated by comparison with experimental data. The pressure distribution and velocity profiles are employed to gain insights into the flow phenomena within manifold systems. This study uses a component employed in the industry. A scientific background has been provided to address an existing real issue. In addition to the reduction in the cross-section, the change in the inlet diameter was investigated. The reduction in the cross-section is carried out gradually instead of using a tapered reduction. Consequently, the process has become more cost-effective by drilling the hole without the need for a turning process.

2. EXPERIMENTAL STUDIES

Figure 3a shows a schematic of the experimental setup, which comprises four main components: the flow system, flow visualization, measurement, and manifold system. In the experiment, the flow system involved pumping water from a reservoir tank using a centrifugal pump. A flowmeter with a measurement range from 0 to 10 ±1.0% l/min was used to measure the liquid flow rate (Q). The experiment was initiated with the lowest flow rate, which was gradually increased by adjusting the valve. The flow rates in each outlet were determined using scaled glass containers, as shown in Fig. 3b. The time taken for fluid to fill the container from each outlet was recorded using a stopwatch, and the water in the containers was then weighed using a precision scale to accurately calculate the flow rates. The flow rate was measured using the container specifically to avoid different pressure drops at each outlet. Otherwise, the pressure difference would prevent accurate flow rate measurement because the flow rate depends on this pressure difference. The sum of the flow rates from the four branches was compared with the measured flow rate of the entire system. The difference was found to be less than 1.5%.

a)

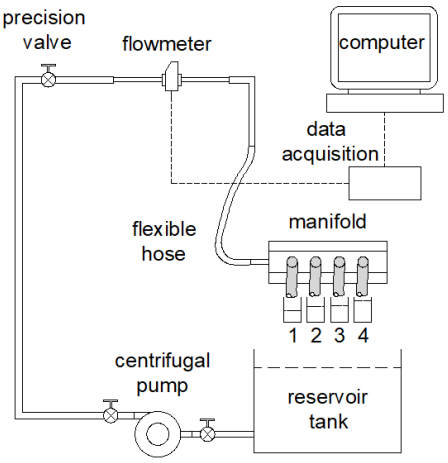

b)

Fig. 3 Experimental setup

3. NUMERICAL STUDIES

Simulations were conducted using the incompressible Navier–Stokes equations within a three-dimensional domain. Star CCM+ software was used for the simulations. The flow analysis was performed assuming single-phase, steady, and turbulent conditions. Reynolds-averaged Navier– Stokes (RANS) equations were solved by employing a realizable two-layer *k-ε* turbulence model to capture the turbulence in the flow.

A first-order implicit scheme was employed to temporally discretize the flow equations. Second-order upwind schemes were used to handle the convective scheme. To prevent nonphysical oscillations in the pressure field, an interpolation scheme on a collocated grid arrangement was implemented, as proposed by Rhie and Chow (1983). The pressure–velocity coupling was carefully handled to ensure convergence and stability during the iterative solution process. The coupling of the pressure and velocity fields in the simulation was effectively and reliably accomplished through the implementation of a suitable coupling algorithm. Specifically, the SIMPLE (Semi-Implicit Method for Pressure-Linked Equations) approach was implemented. This algorithm ensured convergence and precision at every time step during the simulation (Kibar, 2018).

The finite-volume method was employed to solve the governing equations of flow simulations, including the mass and momentum conservation equations. The mass conservation equation is given by Eq. (1).

$$\frac{\partial \rho}{\partial t} + \nabla.\left(\rho \vec{V}\right) \tag{1}$$

In the context of incompressible flow, where the density ρ remains constant (i.e., $\partial\rho/\partial t=0$), the mass conservation equation is simplified as given in Eq. (2).

$$\nabla.\vec{V} \tag{2}$$

This equation ensures that the divergence of the velocity vector $\vec{V}$ is equal to zero, representing the conservation of mass in an incompressible flow.

On the other hand, the momentum conservation equation takes the form:

$$\rho \frac{\partial \vec{V}}{\partial t} + \nabla \cdot \left(\rho \vec{V} \vec{V}\right) = \overrightarrow{f_b} - \nabla p + \nabla \cdot \tau \tag{3}$$

This equation accounts for the changes in momentum in the fluid domain. Here, ρ is the density, p is the static pressure, $\overrightarrow{f_b}$ represents the result of body forces (e.g., gravitational and centrifugal forces), and τ is the viscous stress tensor for Newtonian fluids, as given by Eq. (4):

$$\tau = \mu\left[\left(\nabla \vec{V} + \nabla \vec{V}^T\right) - \frac{2}{3}\nabla \cdot \vec{V} I\right] \tag{4}$$

In Eq. (4), I is the unit tensor and μ is the dynamic viscosity of the liquid. The second term in Eq. (4) captures the effect of volume dilation.

The solver used under-relaxation factors of 0.7, 0.3, and 0.8 for the velocity, pressure, and turbulent kinetic energy, respectively. These factors play a crucial role in ensuring stability and convergence during the solution process.

3.1 Geometric Model and Boundary Conditions

Simulations were performed using the same manifold for two different fitting connections with inside diameters of 20.0 mm (Fig. 4a) and 22.5 mm (Fig. 4b). The side surfaces of the distributor manifold have one inlet channel and four outlet channels, as shown in Fig. 4. The diameter of the main channel is 28 mm. The outlet ducts are fitted with nipples with an inner diameter of 9 mm. The nipples connected to each outlet channel are the same. The main outlet of the manifold is closed with a blind plug, as shown in Fig. 4.

Figure 5 illustrates the boundary conditions applied to the manifold. A mass flow inlet boundary condition is specified to allow liquid entry into the manifold. The pressure outlet boundary condition is defined for each outlet. The inlets and outlets were extended to ensure fully developed flow at the inlet and to prevent backflow at the outlet. These boundary conditions are implemented to accurately simulate the flow behavior within the manifold. The walls of the manifold were defined as no-slip boundary conditions.

Nine computational domains were used in this study, as shown in Fig. 6. First, the original manifold configuration is considered, where the cross-section remains constant along the flow path (Fig. 6a). Then, the

a)

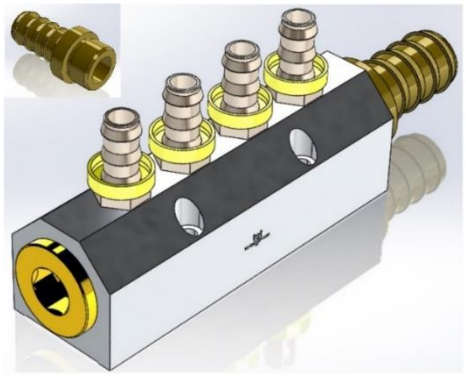

b)

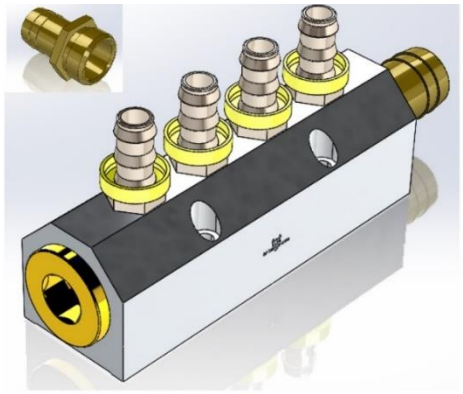

Fig. 4 3D model of the manifolds. a) 20.0 mm and b) 22.5 mm flow entrances

flow cross-section is gradually reduced from the inlet to the outlet (Fig. 6). This reduction was achieved by 2 mm (Fig. 6b), 4 mm (Fig. 6c), and 6mm (Fig. 6d) from the diameter. Fig. 6e shows the case with an inlet diameter of 22.5 mm. In this case, the corners are also 45° chamfered. One of them is given as an example in Fig. 6e. The staging in the other cases is the same, as shown in Fig. 6a–d. The conical tapered manifold recommended in the literature is shown in Fig. 6.

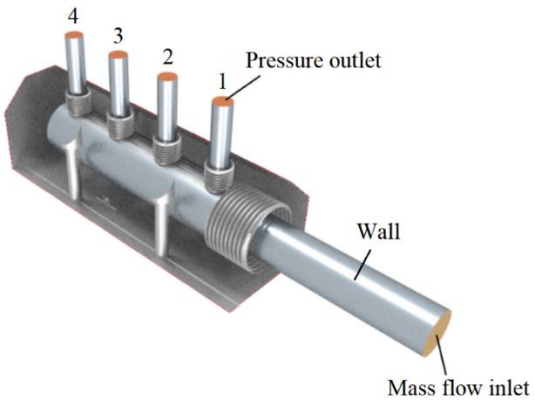

Fig. 5 Boundary conditions

Figure 7 shows the dimensions of the simulation domain. The inlet of the manifold was extended by 100 mm to ensure a fully developed flow. Similarly, the outlets of the manifold were extended by 55 mm from the center to prevent backflow. The diameter of the main duct, whose cross-section remains constant, remains 28 mm along the length of the manifold, as verified by experimental testing. The manifold was gradually reduced in cross-section from the inlet to the outlet to ensure homogeneous outlet flow rates. In the reduced cross-section model, three different models were obtained by reducing the diameter by 2, 4, and 6 mm for each outlet. The dimensions of all models are otherwise identical. The manifolds with a 22.5 mm inlet were identical in dimensions to 2, 4, and 6-mm staggered manifolds. Only the inlet diameters were changed. In the conical tapered model, the same taper was created with a staggered ratio of 1.75. The inlet and outlet diameters were 20 and 9 mm, respectively. The distance between each outlet is 32 mm. Only the diameter values in sections D1, D2, D3, and D4 were changed. These values are presented in Table 1.

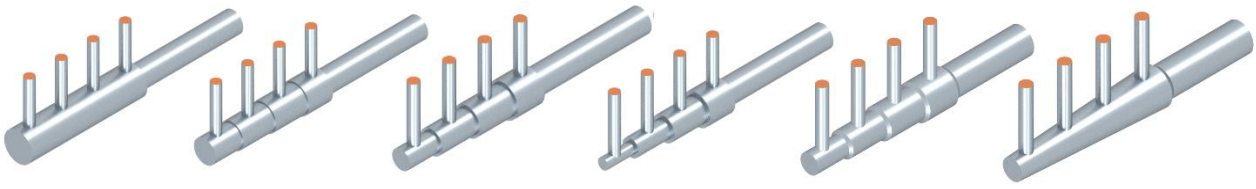

a) b) c) d) e) f)

Fig. 6 Computational models of the manifolds: a) straight, b) 2 mm, c) 4 mm, d) 6 mm gradually reduced, e) 22.5 mm entrance, and f) conical tapered

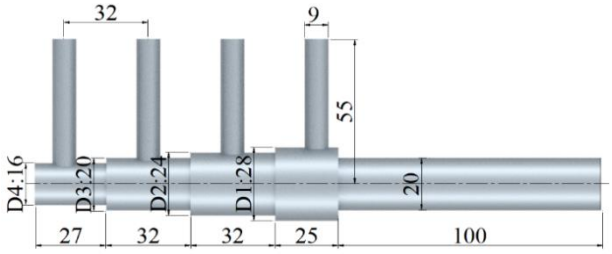

Fig. 7 Dimensions of the 1.75-ratio staggered manifold domain

Table 1 Dimensions of the manifolds

Case	Staggered ratio (D1/D4)	D1 (mm)	D2 (mm)	D3 (mm)	D4 (mm)
Straight	1	28	28	28	28
Conical tapered	1.75	28	-	-	16
2 mm	1.27	28	26	24	22
4 mm	1.75	28	24	20	16
6 mm	2.8	28	22	16	10

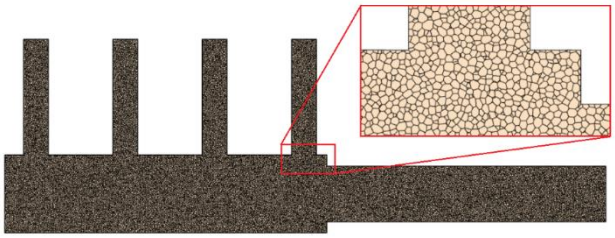

Fig. 8 Mesh structure of the manifold domain

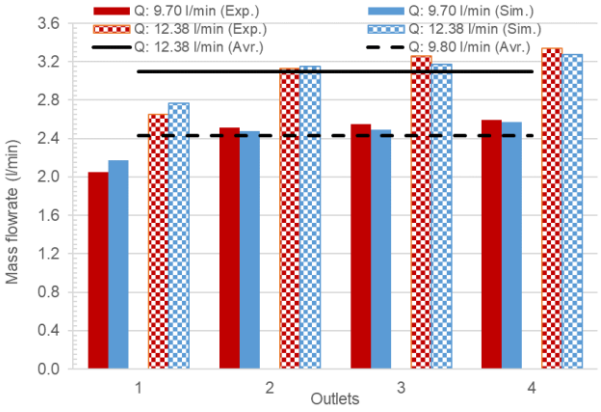

Fig. 9 Liquid flow rates from each outlet of the straight manifold, *Q: 9.70* l/min and 12.38 l/min

3.2 Mesh Domain

Polyhedral cells were used to create the mesh, as shown in Fig. 8. The mesh consisted of 875,000 cells, which is a suitable number for the size and complexity of the geometry being simulated. On the basis of the outlet flow rates obtained from the experiment, a mesh independence study was performed, which revealed that this value was significantly higher than the number of meshes that could optimally provide the flow.

It is necessary to check the network quality to ensure the accuracy of the simulation results. Two important criteria for mesh quality are aspect ratio and skewness. The aspect ratio is the ratio of the longest edge of a cell to the shortest edge, and skewness is a measure of how distorted a cell is. Both criteria should be within acceptable limits to ensure accurate simulation results. In this study, the aspect ratio and skewness were within acceptable limits. Another important aspect of meshing is the resolution of the boundary layers. The boundary layer is a thin layer of fluid near the surface of a solid object, where viscous effects are important. The y^+ value was maintained between 0 and 30 throughout this study to ensure accurate resolution of the boundary layer.

4. RESULTS AND DISCUSSION

Figure 9 shows the flow rates of the liquid exiting each outlet of the straight manifold at two different inlet flow rates. A comparison between the experimental and numerical results reveals an almost close agreement. The most significant disparity between the experimental and simulation data is observed at the first outlet, with a difference of 5.07%. Variances in the other outlets' values range between 0.6% and 3.1%. It can be inferred that the experimental and simulation results are consistent and compatible.

As shown in Fig. 9, when the flow rate at each outlet is equal, the graph represents the average flow rate that should be taken from each outlet. The flow rate at the 1st outlet is below the average flow rate, whereas the flow rates at the other outlets are above the average flow rate. The highest flow rate among the manifold outlets is observed at the 4th outlet, which is the last outlet in the sequence. Subsequently, relatively high flow rates are observed at the 3rd and 2nd outlets, respectively. The flow rates at the 2nd and 3rd outlets are relatively close to the average flow rate. Consequently, it can be concluded that most flow is directed toward the 4th (last) outlet, while the 1st outlet receives the lowest flow rate in the straight manifold case.

In Fig. 10, the outlet flow rates are presented as 3D graphs for different inlet flow rates. Gradually decreasing the diameters of the main distribution section results in slight homogenization of the flow rates with each staggered reduction. This homogenization continues to some extent up to a 1.75-ratio staggered manifold, as shown in Fig. 10c. However, beyond the 1.75-ratio staggered manifold, homogenization is further disrupted, as shown in Fig. 10d, which shows the 2.80-ratio staggered manifold. Across the straight, 1.27, and 1.75 ratio staggered manifolds, the highest flow rate emerges at the 4th outlet. Conversely, the 4th outlet experiences the lowest flow rate within the 2.80 ratio staggered manifold. Likewise, in the other scenarios, the 1st outlet consistently records the lowest flow rate, except in the case of the 2.80 ratio staggered manifold, where the second-highest flow rate occurs at the 1st outlet. It is concluded that it is very important to carefully consider the stage ratio so that the gradual reduction of the manifold diameter contributes to the homogeneity of the outlet flows.

The outcomes of scenarios where the liquid enters the manifold with a slightly larger diameter (22.5mm) are shown in Fig. 11. In Fig. 11a, concerning the straight manifold configuration, it is evident that aligning the inlet diameter of the liquid closely with the manifold's inlet

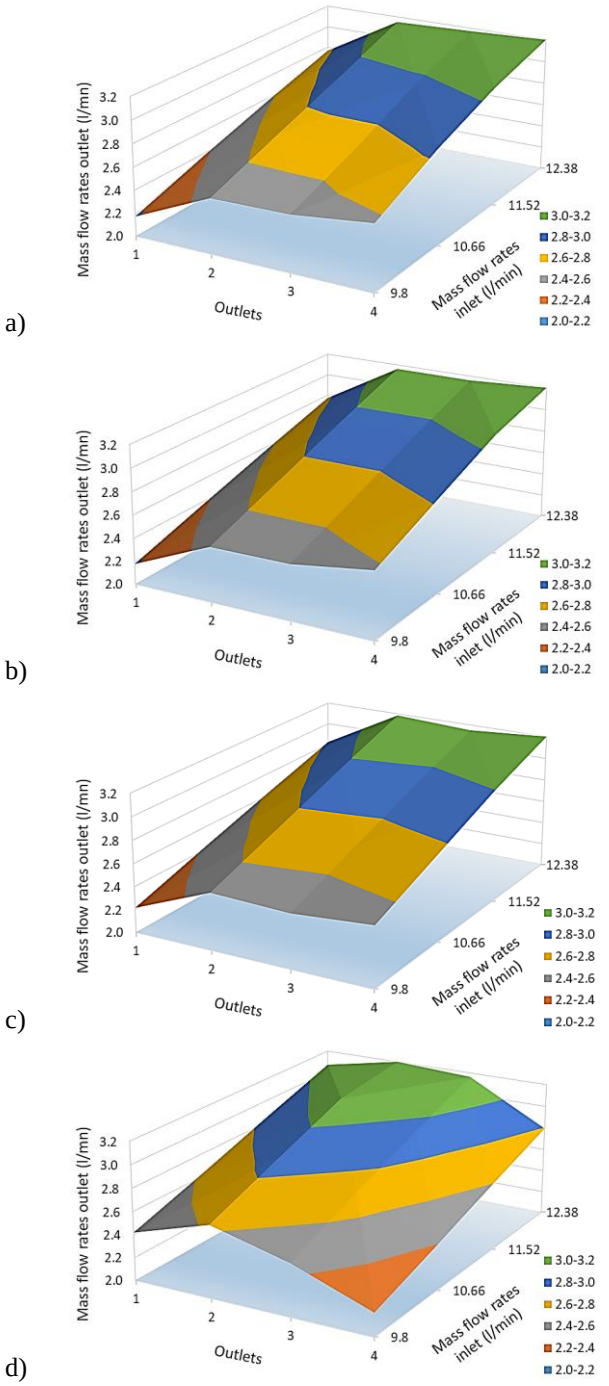

Fig. 10 a) Straight, b) 1.27, c) 1.75, and d) 2.80 ratio staggered manifolds

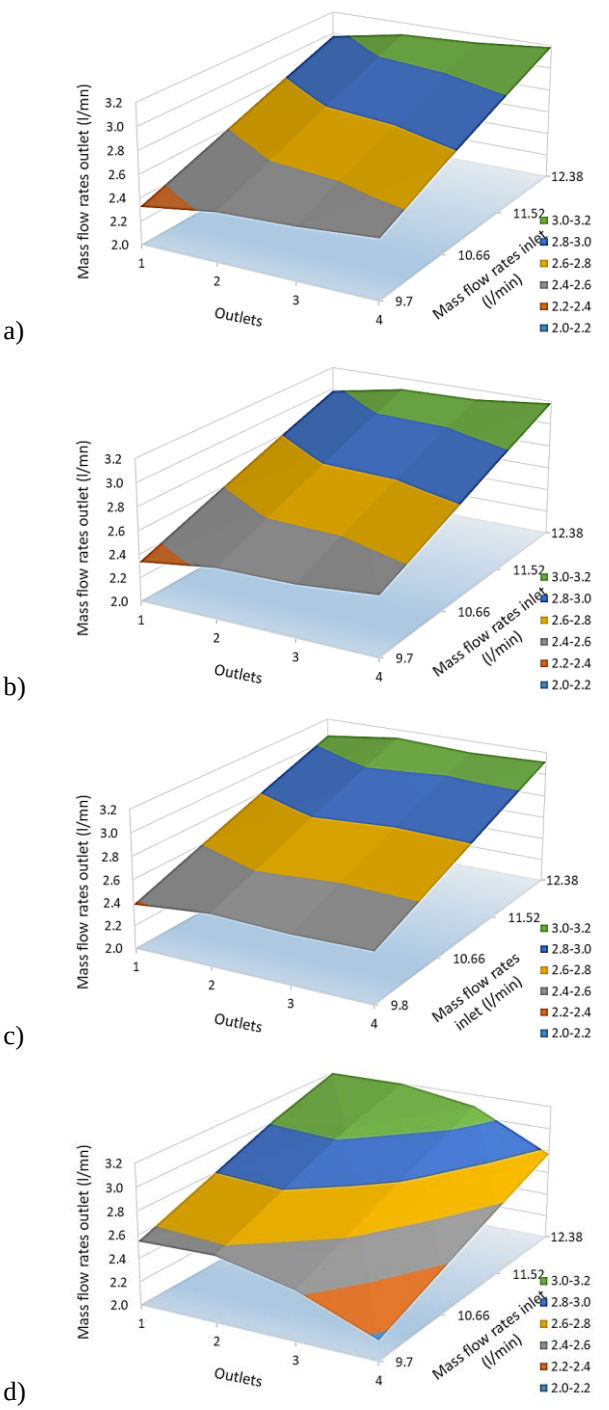

Fig. 11 a) Straight, b) 1.27, c) 1.75, and d) 2.80 ratio staggered manifolds

diameter promotes a more uniform distribution of flow rates across the outlets. This homogeneity is enhanced when employing a 1.27-ratio staggered manifold, as depicted in Fig. 11b. Notably, the highest level of outlet homogeneity is achieved when using a 1.75-ratio staggered manifold, as shown in Fig. 11c. In contrast, Fig. 11d illustrates that the uniformity in flow rates is markedly disrupted as the staggered ratio is further augmented (2.38 ratio). In this instance, the highest flow rate occurs at the first outlet, followed by progressively diminishing flow rates at the second, third, and fourth outlets. The fourth outlet registers an exceedingly low flow rate. Taken together, these results underscore that aligning the liquid inlet diameter closely with the manifold's inlet diameter or employing a moderately staggered ratio (around 1.75) substantially contributes to achieving more uniform flow rates across the outlets. Conversely, escalating the staggered ratio beyond a certain threshold (2.38 ratio staggered under the conditions of this article) leads to a substantial deterioration in the homogeneity of the flow distribution.

In the case of a straight manifold, the lowest outlet flow rate is observed at outlet 1, whereas the highest outlet flow rate is recorded at outlet 4. Therefore, a comparison of the flow rates at outlets 1 and 4 is specifically examined in Fig. 12 for two distinct inlet diameters, including 20.0 and 22.5 mm. Notably, as the inlet flow rate increases, the

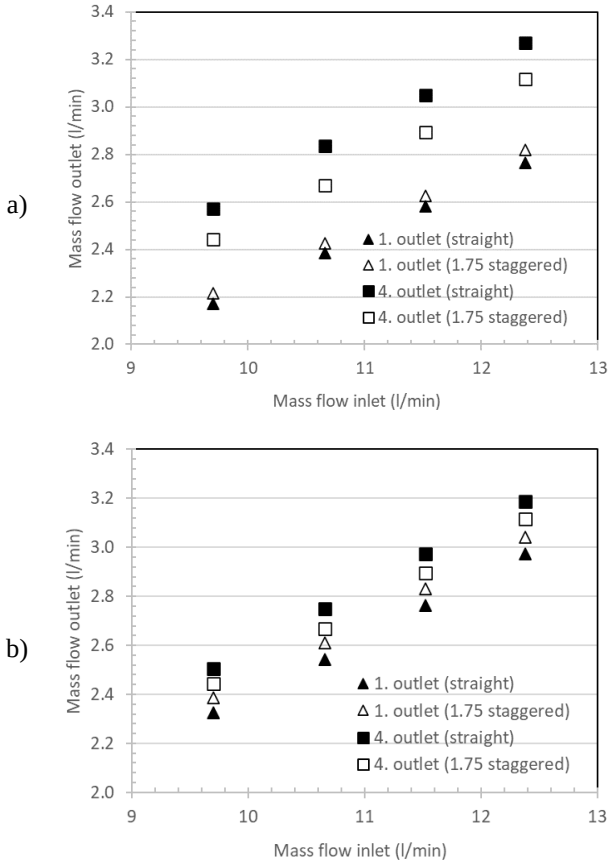

Fig. 12 Mass flow outlets for 1st and 2nd outlets with a) 20.0 mm and b) 22.5 mm inlet diameters, *Q*: 9.7 l/min

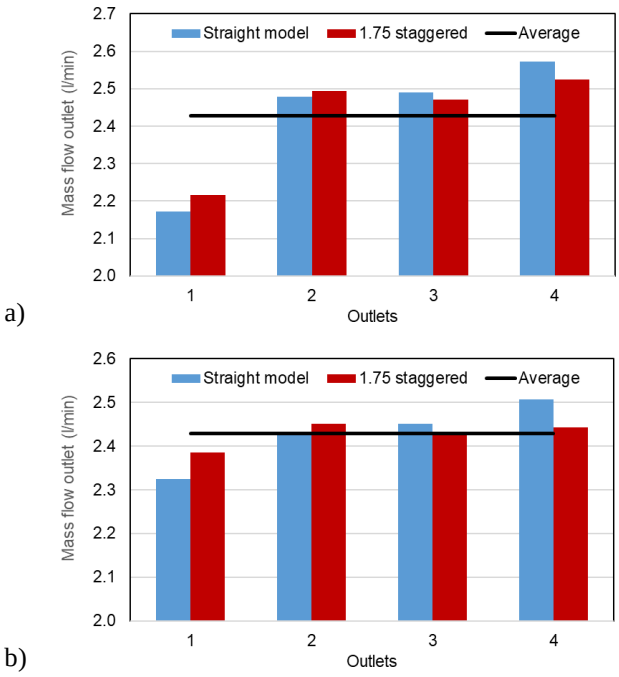

Fig. 13 Mass flow outlets for straight and 1.75 ratio-staggered manifolds. a) 20.0 mm b) 22.5 mm, *Q: 9.7* l/min

outlet flow rates exhibit almost linear augmentation. For the straight manifold, significant flow rate disparities are evident between outlets 1 and 4 across all inlet flow rates for the 20 mm inlet diameter case, as depicted in Fig. 12a. While this disparity slightly decreases for the first outlet, there is a notable reduction for the fourth outlet. For a 22.5 mm inlet diameter in the straight manifold, the differences in flow rates between outlets 1 and 4 are lower than those for the 20 mm inlet diameter case, as shown in Fig. 12b.

Furthermore, these discrepancies are further diminished when a 1.75 ratio staggered manifold is used. The outcomes imply that regardless of variations in the inlet flow rate, achieving a balanced flow distribution between outlets 1 and 4 is optimally realized by employing a manifold with an inlet diameter closely aligned with the liquid inlet coupled with a staggered ratio of 1.75. In summary, these findings underscore the pivotal role played by the manifold inlet diameter and the selection of a suitable staggered ratio (1.75) in attaining a more uniform flow distribution.

Figures 13a and 13b show the results for both straight and 1.75 ratio staggered manifolds with inlet diameters of 20.0 and 22.5 mm, respectively. In the case of the straight manifold, the flow rate at outlet 1 is substantially lower than that at the other outlets. Conversely, outlet 4 exhibited the highest flow rate among all outlets. Meanwhile, the flow rates at outlets 2 and 3 are relatively close to each other. At outlet 1 in the straight manifold, the flow rate is considerably lower than the expected average flow rate for all outlets. However, the flow rates at the other outlets are above the average flow rate. In the 1.75 manifold, the lowest flow rate is observed at outlet 1. Despite this, all outlets show flow rates close to the average flow rate. This indicates that the 1.75 ratio staggered manifold design effectively balances the flow distribution across all outlets, resulting in improved performance compared with the straight manifold. The results indicate the superiority of the 1.75 ratio staggered manifold configuration in achieving a more even flow rate distribution between outlets. The flow rates at the middle outlets (outlets 2 and 3) are close to the average value, which demonstrates the effectiveness of this design in maintaining a balanced flow distribution in these regions. However, the most critical condition occurs at the first and last outlets. The flow rate at the first outlet is considerably lower than the average, whereas the flow rate at the last outlet is also affected, resulting in a deviation from the average.

Figure 14 shows the flow rates at the outlets of the 1.75 ratio conical tapered manifold recommended in the literature for outlet uniformity (Tong et al., 2009; Hassan et al., 2014b; Karali et al., 2022). As depicted in Fig. 14a, nearly the same mass flow output is achieved in the first three outlets, with a slight increase. Although there is a slight increase in the fourth outlet, the flow rates at all the outlets remain close to each other. In Fig. 14b, a comparison is made between the flow rates at the outlets of the tapered manifold and the staggered manifold with a ratio of 1.75, which was identified as the best case in this study. In the conical tapered manifold, there is an approximately linear increase in output throughout the flow. In the staggered manifold, a fully linear increase is not observed. The flow rates at the first and third outlets in both cases are approximately the same. In the conical

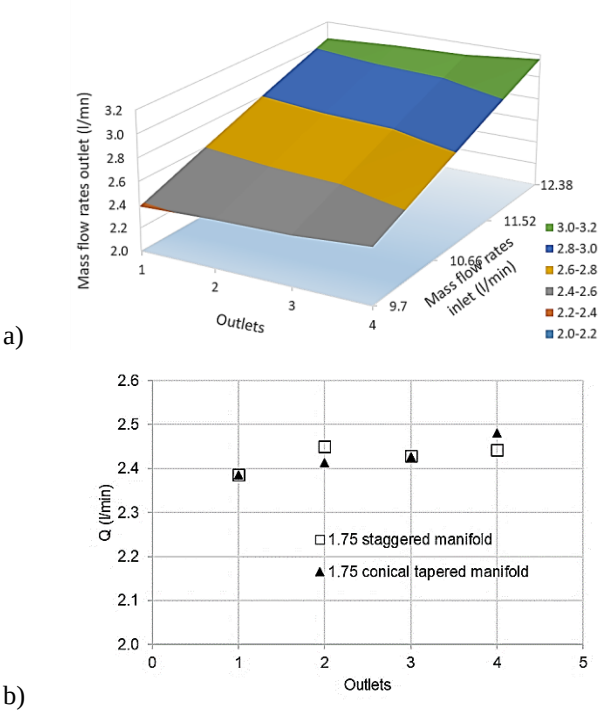

Fig. 14 Outlet flow rates of the conical tapered manifolds a) all flow rates and b) *Q*: 9.70 l/min flow rates

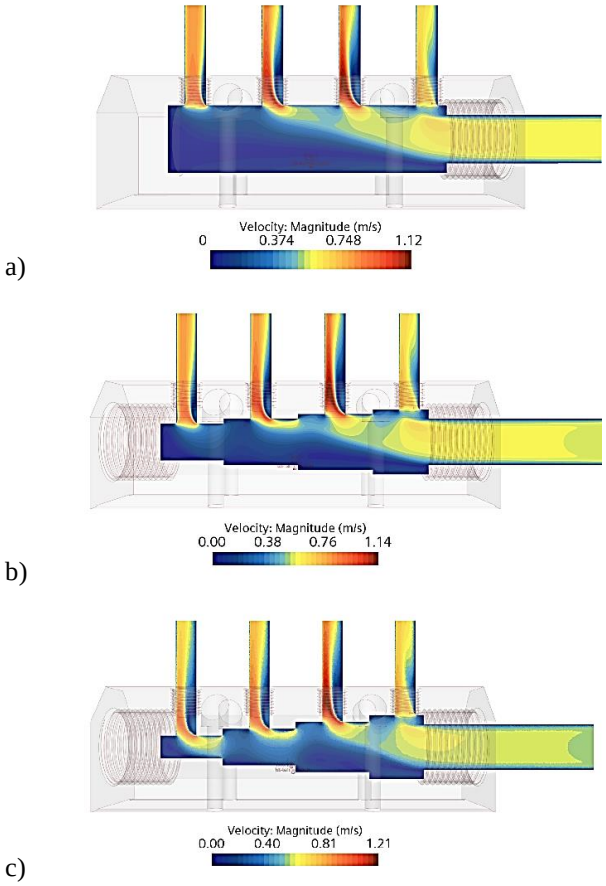

Fig. 15 Velocity contours at the midplane of the manifolds. a) Straight, b) 1.75, and c) 2.80 ratio staggered manifolds. 20 mm inlet diameter

tapered case, the highest flow rate is obtained at the fourth outlet, whereas in the staggered manifold, the highest output flow rate is achieved at the second outlet, as shown in Fig. 14b. Although the staggered manifold outlet uniformity does not exhibit a linear trend like the conical tapered manifold, the result is as good as that of the conical tapered manifold.

In Fig. 15, velocity contours at the middle plane of the manifold with a 20 mm inlet are presented. The liquid flow is concentrated in the vicinity of the outlets, whereas in other regions, the liquid remains almost stagnant or flows at very low velocities. Flow separations are observed at all outlets, leading to the formation of vortices in these regions. These vortices cause flow disruptions and result in a consequent pressure drop (Korkmaz et al., 2022). In the straight manifold (Fig. 15a), because of the negligible flow separation and low-pressure drop, the highest flow rate occurs at the 4th outlet. Maximum flow velocities are observed at the middle outlets (outlets 2 and 3). However, larger vortices are formed in these regions, which can negatively impact the flow distribution. In the worst-case scenario, which is the 2.80 ratio manifold (Fig. 15c), a decrease in flow velocity occurs at the last outlet (outlet 4), accompanied by the formation of a larger vortex. Consequently, a significant pressure drop occurs in this region, leading to a smaller amount of liquid directed to the 4th outlet. These flow separations and vortices adversely affect the flow distribution, causing pressure losses and uneven flow rates at the outlets.

In Fig. 16, the velocity contours along the flow direction are presented for straight, 1.75 ratio staggered, and conical tapered manifolds. A significant velocity gradient is observed for the 20 mm inlet manifold, as shown in Fig. 16a, where higher liquid velocities occur along the flow at the manifold outlet regions. In contrast, the 22.5 mm inlet manifold shows a more homogeneous velocity gradient, leading to more uniform outlet flow velocities. When both cases are staggered, homogeneity is further increased, as shown in Fig. 16b. The lower inlet diameter, particularly in the regions opposite the outlets, results in almost stagnant liquid flow. However, with staggered manifolds, this stagnant region is reduced slightly, and the flow is directed toward the outlets, improving flow homogeneity in the 20 mm inlet manifold. Nevertheless, complete homogeneity cannot be achieved, especially in the regions where the flow enters the manifold. Conversely, in the 22.5 mm inlet manifold with staggering, the flow is nearly perfectly homogenized, with almost no stagnant liquid regions on the opposite side of the outlets.

Stalling effectively directs the flow toward the outlets, ensuring a more balanced and efficient flow distribution. The findings indicate that the choice of inlet diameter and appropriate staggering significantly influence the flow behavior and homogeneity in the manifold. Additionally, it is worth noting that using a 22.5mm inlet with a 1.75 ratio staggered manifold, as recommended in the literature for a conical tapered manifold, results in approximately the same flow velocities along the flow direction, as shown in Fig. 16c. A well-designed staggered manifold with a diameter close

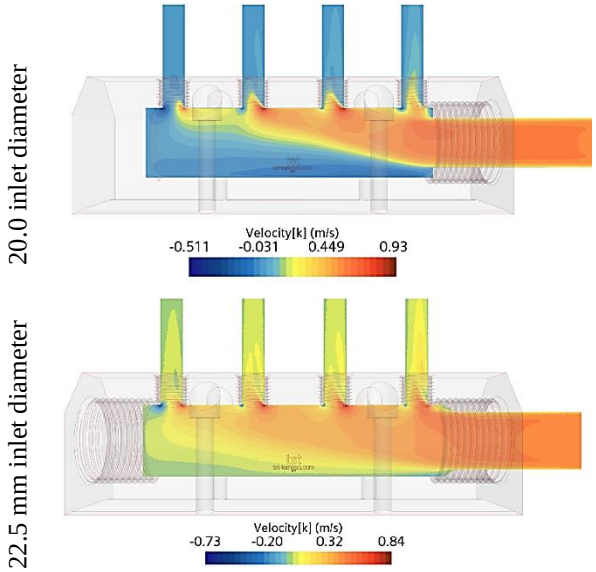

a) Straight manifold

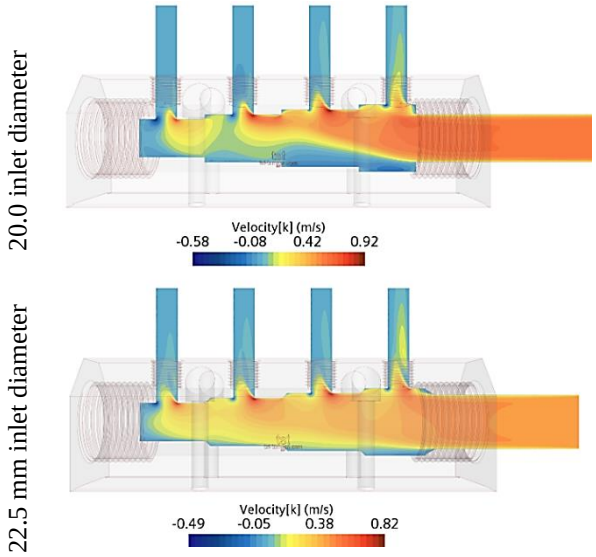

b) 1.75 ratio staggered manifold

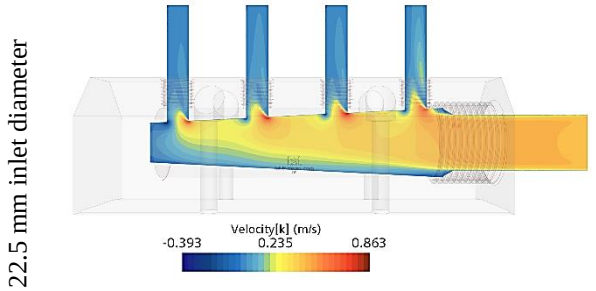

c) Conical tapered manifold

Fig. 16 Velocity contours at the midplane of the manifolds. a) Straight, b) 1.75 ratio staggered, and c) conical tapered manifolds

to or the same as the manifold inlet diameter provides improved flow distribution and minimizes stagnant flow regions, resulting in enhanced performance.

Figure 17 illustrates the manifold with a staggered ratio of 2.80, which displays the poorest homogeneous

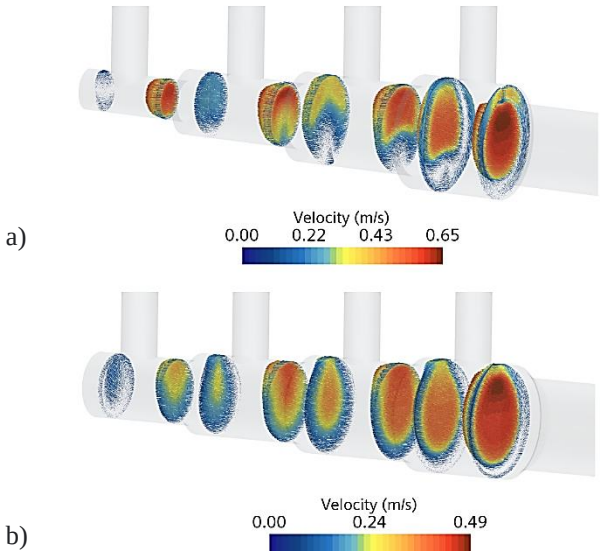

Fig. 17 Velocity vectors across the cross-section. *Q*: 0.1618 kg/s, 2.8 ratio, and 1.758 ratio manifolds

flow distribution (Fig. 17a), and the manifold with a staggered ratio of 1.75 showcasing the best homogonies flow distribution (Fig. 17b). In the manifold with a ratio of 1.75, there is a slight improvement in uniformity. After the first outlet, in the manifold with a ratio of 2.28, the flow velocities are higher toward the middle and outlet. This nonuniform flow distribution remains relatively consistent as the cross-section narrows. Beyond the second outlet, there is a substantial drop in the flow velocity, resulting in a more concentrated flow distribution at the exit region. After the third outlet, the fluid velocity further decreases, followed by an increase in the final stage. This leads to irregular velocities the entire flow. Within the manifold with a ratio of 1.75, in the inlet section, the flow velocity is notably higher in the middle, whereas significantly lower flow velocities occur at the edges. Subsequently, flow uniformity is predominantly maintained the entire flow. This uniformity is minimally disrupted in sections after stage transitions and outlets. Thus, these findings highlight that by ensuring uniform flow throughout the distributor manifold, equal flow rates can be achieved at the outlets.

Dean vortices, a fluid dynamics phenomenon, are characterized by the formation of helical vortical structures in curved pipe flows (Dean, 1927). These vortices arise due to the centrifugal and Coriolis forces acting on the fluid within the curved geometry of the manifold. The centrifugal force tends to push the fluid toward the outer curvature, whereas the Coriolis force induces rotation of the fluid, thereby creating two counter-rotating roll regions (Kalpakli Vester et al., 2016). Dean vortices, representing a characteristic fluid flow pattern, consistently manifest at the outlets of the manifold. Notably, each of the four outlets exhibits a near-identical formation of Dean vortices, indicating a uniform and consistent occurrence across the manifold system, as illustrated in Fig. 18. This formation initiates as soon as the fluid enters the outlet arms and continues to develop toward the outlets.

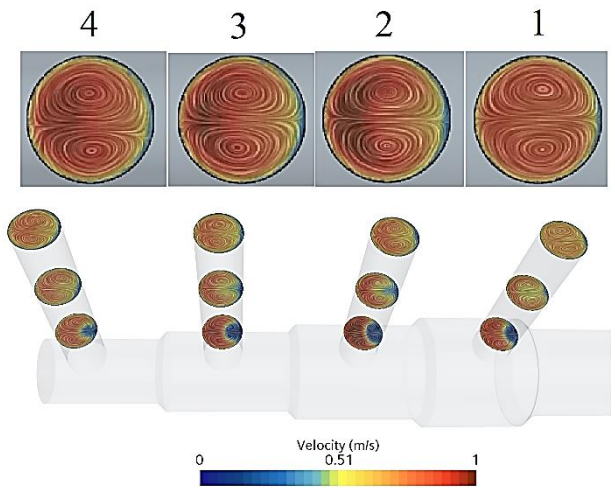

Fig. 18 Dean vortices at the outlets for 1.758 ratio manifolds, *Q*: 0.1618 kg/s

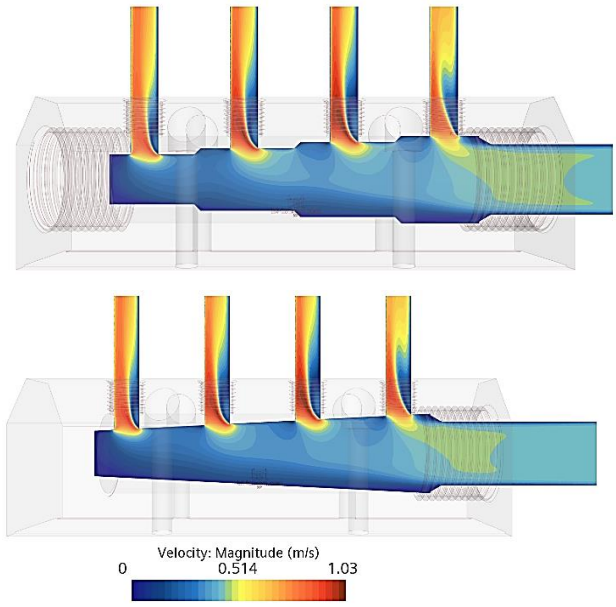

Fig. 19. Velocity contours at the midplane of the manifolds. a) 1.75 ratio staggered and b) conical tapered manifolds.

Figure 19 depicts the stagnation velocity regions occurring when the liquid enters the branches of the manifold. Detailed flow separations of the 1.75 ratio staggered manifold and the conical tapered manifold at mid-plane velocity contours are illustrated in Fig. 19. In both cases, maximum velocities are observed at nearly the same values. The fluid directed to the outlet branches exhibits extremely similar behavior in both cases, with flow separations being comparable at each outlet. Consequently, similar values are obtained at the outputs of both the 1.75 ratio stage and the conical tapered manifold.

5. CONCLUSION

The distributor manifold is an important component in hydraulic systems that distribute fluid flow. However, in some cases, nonuniform flow distribution may occur between branches. In this study, different manifold designs are investigated using both experimental and numerical methods to achieve uniform flow distribution in the manifold. Initially, the flow rate differences between the distribution branches were analyzed using a straight manifold. Subsequently, a gradually decreasing manifold design was employed to explore the impact on flow rate variations among distribution arms. Two different diameters were used as the inlet diameters. The main objective of this study is to achieve uniform flow rates for all distribution branches in the distributor manifold system. A single inlet and four outlet manifolds are used for this purpose.

- The flow rate differences between the distribution branches can be effectively reduced by designing the manifold with a gradually decreasing configuration. This gradually decreasing design ensures a more uniform distribution of fluids in each distribution branch. Compared with the straight manifold design, the gradually decreasing manifold allows the fluid to flow at lower velocities in regions encountering resistance, thereby minimizing flow rate discrepancies.
- The importance of considering the distributor manifold geometry to achieve flow rate uniformity is emphasized. In this context, it is concluded that a manifold design with a gradually decreasing cross-section will enhance system performance by providing a more balanced flow distribution.
- When the liquid inlet diameter is maintained close to the manifold's inlet diameter and combined with a 1.75 ratio staggered design, a more uniform and efficient distribution of fluid flow among the outlet channels is achieved.
- Maintaining the liquid inlet diameter close to the manifold's inlet diameter, combined with the stepped design featuring a ratio of 1.75, ensures a more uniform distribution of liquid flow between the outlet channels.
- The results suggest that the staggered manifold can achieve almost the same uniform flow branching as the conical tapered manifold recommended in the literature. Despite differences in the flow patterns, the staggered manifold demonstrates comparable outlet uniformity, indicating that similar performance can be achieved with a manifold with a faster and cheaper production process.

CONFLICT OF INTEREST

The authors have no conflicts of interest to declare.

AUTHORS CONTRIBUTION

Fathi Yazici: investigation; **Muhammet Ali Karadag**: software and formal analysis; **Pinar Gokluberk**, conceptualization and methodology; **Ali Kibar**: Writing, reviewing, and editing.

REFERENCES

Acrivos, A., Babcock, B. D., & Pigford, R. L. (1959). Flow distributions in manifolds. *Chemical Engineering Science*, *10*(1–2), 112–124. https://doi.org/10.1016/0009-2509(59)80030-0

Bajura, R. A. (1971). A Model for flow distribution in manifolds. *Journal of Engineering for Power*, *93*(1), 7–12. https://doi.org/10.1115/1.3445410

Bajura, R. A., & Jones, E. H. (1976). Flow distribution manifolds. *Journal of Fluids Engineering*, *98*(4), 654–665. https://doi.org/10.1115/1.3448441

Choi, S. H., Shin, S., & Cho, Y. I. (1993). The effect of area ratio on the flow distribution in liquid cooling module manifolds for electronic packaging. *International Communications in Heat and Mass Transfer*, *20*(2), 221–234. https://doi.org/10.1016/0735-1933(93)90050-6

Dean, W. R. (1927). XVI. Note on the motion of fluid in a curved pipe. *The London, Edinburgh, and Dublin Philosophical Magazine and Journal of Science*, *4*(20), 208–223. https://doi.org/10.1080/14786440708564324

Hassan, J. M., Mohamed, T. A., Mohammed, W. S., & Alawee, W. H. (2014a). Modeling the uniformity of manifold with various configurations. *Journal of Fluids*, *2014*(ID:325259), 1–8. https://doi.org/10.1155/2014/325259

Hassan, J. M., Mohamed, T. A., Mohammed, W. S., & Alawee, W. H. (2015). Experimental and Numerical Study on the Improvement of Uniformity Flow for Three-Lateral Dividing Manifold. *EIIC International Journal of Engineering and Technology*, *12*(1), 29–37.

Hassan, J. M., Mohammad, W. S., & Hameed, A. F. (2012). Study of three dimensional fluid flow inmanifold-laterals system study of three dimensional fluid flow in manifold-laterals system. *Engineering and Technology Journal*, *30*(7), 1132–1148. http://dx.doi.org/10.30684/etj.30.7.3

Hassan, J. M., Mohammad, W. S., Mohamed, T. A., & Alawee, W. H. (2014b). CFD simulation for manifold with tapered longitudinal section. *International Journal of Emerging Technology and Advanced Engineering*, *4*(2), 8. www.ijetae.com

Jiang, Y., Alawee, W. H., Essa, F. A., Abdullah, A. saad, Omara, Z. M., Ahmad, H., Ali, R., Wang, F., & Menni, Y. (2022). Effect of area ratio and Reynolds number on the distribution of discharge in dividing manifold. *International Journal of Low-Carbon Technologies*, *17*(May 2022), 1271–1279. https://doi.org/10.1093/ijlct/ctac018

Kalpakli Vester, A., Sattarzadeh, S. S., & Örlü, R. (2016). Combined hot-wire and PIV measurements of a swirling turbulent flow at the exit of a 90° pipe bend. *Journal of Visualization*, *19*(2), 261–273. https://doi.org/10.1007/s12650-015-0310-1

Karali, M. A., Alharthi, M. A., & Refaey, H. A. (2022). Influence of using different tapered longitudinal section manifolds in a Z shaped flat plate solar collector on flow distribution uniformity. *Case Studies in Thermal Engineering*, *33*, 101922. https://doi.org/10.1016/J.CSITE.2022.101922

Kee, R. J., Almand, B. B., Blasi, J. M., Rosen, B. L., Hartmann, M., Sullivan, N. P., Zhu, H., Manerbino, A. R., Menzer, S., Coors, W. G., & Martin, J. L. (2011). The design, fabrication, and evaluation of a ceramic counter-flow microchannel heat exchanger. *Applied Thermal Engineering*, *31*(11–12), 2004–2012. https://doi.org/10.1016/J.APPLTHERMALENG.2011.03.009

Kibar, A. (2018). Experimental and numerical investigation on a liquid jet impinging on a vertical superhydrophobic surface: spreading and reflection. *Progress in Computational Fluid Dynamics, An International Journal*, *18*(3), 150–163. https://doi.org/10.1504/PCFD.2017.10004671

Korkmaz, Y. S., Kibar, A., & Yigit, K. S. (2022). Experimental and numerical investigation of fluid flow in hydraulic filters. *Journal of Applied Fluid Mechanics*, *15*(2), 363–371. https://doi.org/10.47176/jafm.15.02.32898

Korkmaz, Y. S., Kibar, A., & Yiğit, K. S. (2021). Experimental and numerical investigation of flow in hydraulic elbows. *Journal of Applied Fluid Mechanics*, *14*(4), 1133–1146. https://doi.org/10.47176/jafm.14.04.32243

Mazaheri, N., Bahiraei, M., & Razi, S. (2022). Second law performance of a novel four-layer microchannel heat exchanger operating with nanofluid through a two-phase simulation. *Powder Technology*, *396*, 673–688. https://doi.org/10.1016/j.powtec.2021.11.021

Minocha, N., & Joshi, J. B. (2020). 3D CFD simulation of turbulent flow distribution and pressure drop in a dividing manifold system using openfoam. *International Journal of Heat and Mass Transfer*, *151*, 119420. https://doi.org/10.1016/J.IJHEATMASSTRANSFER.2020.119420

Rhie, C. M., & Chow, W. L. (1983). Numerical study of the turbulent flow past an airfoil with trailing edge separation. *AIAA Journal*, *21*(11), 1525–1532. https://doi.org/10.2514/3.8284

Siddiqui, O. K., Al-Zahrani, M., Al-Sarkhi, A., & Zubair, S. M. (2020). Flow distribution in U- and Z-Type manifolds: Experimental and numerical investigation. *Arabian Journal for Science and Engineering*, *45*(7), 6005–6020. https://doi.org/https://doi.org/10.1007/s13369-020-04691-4

Tarodiya, R., Khullar, S., & Gandhi, B. K. (2020). CFD modeling of multi-sized particulate slurry flow through pipe bend. *Journal of Applied Fluid Mechanics*, *13*(4), 1311–1321.

https://doi.org/10.36884/JAFM.13.04.31066

Tomor, A., & Kristóf, G. (2016). Validation of a discrete model for flow distribution in dividing-flow manifolds: Numerical and experimental studies. *Periodica Polytechnica Mechanical Engineering*, *60*(1), 41–49. https://doi.org/10.3311/PPme.8518

Tong, J. C. K., Sparrow, E. M., & Abraham, J. P. (2009). Geometric strategies for attainment of identical outflows through all of the exit ports of a distribution manifold in a manifold system. *Applied Thermal Engineering*, *29*(17–18), 3552–3560. https://doi.org/10.1016/j.applthermaleng.2009.06.010